A PRECISE MAGNETIC BEARING EXCITER FOR ROTORDYNAMIC EXPERIMENTS

Conrad Gähler

International Center for Magnetic Bearings, ETH Zurich, Switzerland

Peter Förch

Arbeitsgruppe Maschinendynamik, Universität Kaiserslautern, Germany

ABSTRACT

An AMB configuration for rotor dynamic experiments is described. It allows precise test force generation while keeping the rotor floating. As the force is the primary control variable, the position is considered mainly as a disturbance input.

This results in the need for new concepts: In order to achieve the desired force precision, the force is measured with Hall effect sensors. A novel geometry, a novel AMB modelling method, force computation method, and multi-level digital controller structure have been developed for this purpose. The whole system can be conveniently controlled through a MATLAB interface. It thus offers new possibilities for rotor dynamic experiments.

The novel modelling method yields important new results also for conventionally used bearing geometries.

1. INTRODUCTION

Overall project, motivation

Many investigations exist on the vibrational behaviour of rotating rotors, as well as on the vibrational behaviour of non-rotating structures, e.g. flexible foundations. However, little work has been done on the combination of both, i.e. rotating rotors on flexible foundations. Such knowledge is essential for predicting performance, stability, vibration levels, and fatigue of rotating machinery. It is the goal of the BRITE/EURAM project MARS[1] (Modal Analysis of Rotating Structures) of the European Community to further develop the theory in this field and to validate the results experimentally.

In general, combined rotating/non-rotating systems must be described by periodically time varying differential equations [1]. In the MARS project, the following methods shall in particular be developed for combined rotating/non-rotating structures:

- FE modelling
- measuring the frequency response function (FRF) with non-contacting excitation and measurement
- modal analysis
- updating of FE model based on FRF measurements

The contribution of the International Center for Magnetic Bearings (ICMB), Zurich, consists in building a Magnetic Bearing Exciter/Bearing system that is tailored to the needs for rotor dynamic experiments. Moreover, it is involved in the development of the overall test rig.

Contact-free excitation

Various techniques for excitation of rotating rotors have been applied [2]: Excitation by impact hammer; shaking the rotor through a shaft rider; transmitting unbalance forces from a second rotor, and others. The use of magnetic bearings has been described in [3,4].

AMB excitation allows contact-free generation of forces with arbitrary time history on the rotating rotor. The approach described in this paper reduces the sensitivity with respect to many parameters. Within the framework of MARS, an AMB specially tailored to testing purposes in rotor dynamics has been designed. Thanks to its special measurement system, its sophisticated multi-level digital control and its interface to the standard mathematics program MATLAB, it offers a number of completely new features.

Organisation of the paper

In section 2, the experiments planned in the MARS project are described. The requirements of the AMB configuration then follow. Section 3 deals with modelling radial AMBs. Conventional AMB models do not consider magnetic coupling between the pole pairs. It is shown, however, that such couplings must be considered for precise modelling. Therefore, a two-dimensional model of the AMB is established. Different possible AMB con-

---

[1] BRITE/EURAM project nr. 5464.-92. Full title: "Development of Validated Structural Dynamic Modelling and Testing Techniques for Vibration Predictions in Rotating Machinery". The project partners are

- Imperial College, London, UK (Prof. D. Ewins)
- University of Kaiserslautern, D (Prof. R. Nordmann)
- ETH Zurich (Prof. G Schweitzer)

figurations are compared in section 4. Finally, the controller structure is presented in section 5.

2. SPECIFICATIONS OF THE DESIGN OF THE MAGNETIC BEARING EXCITER

Test rig and planned experiments

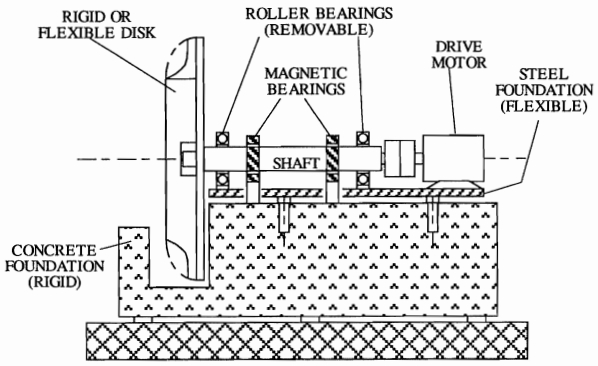

FIGURE 1: Outline of the test rig

Figure 1 shows an outline of the test rig. Its rotor mass is 41 kg, including the disc mass of 17 kg. The rotor length is about 1 m.
Dynamic tests in different mechanical structures will be carried out. These structures include

- rigid or flexible rotor
- rigid or flexible disc attached to the rotor
- rotating or non-rotating rotor
- rotor supported by magnetic bearings (which act as exciters at the same time), or by roller bearings (with AMB's acting only as exciters)
- roller bearings mounted on a rigid or on a flexible foundation

In all cases, sinusoidal excitation must be provided. The excitation forces in the four axes match exactly the user-defined frequency as well as the user-defined amplitudes and relative phase shifts between the four axes. It is also possible to excite the rotor synchronously with the rotor revolution, using a synchronisation pulse from the motor.

Key figures of the magnetic bearing exciter

- Maximum force: $F_{max} = 800$ N
- Dynamic force: Sinusoidal forces with amplitude F_{max} can be achieved up to 200 Hz
- Inner Stator diameter: 116 mm
- Nominal air gap: $s_0 = 0.8$ mm

Digital control and MATLAB interface

The AMB exciter is controlled by a TI TMS 320C25 digital signal processor board from Mecos Traxler AG. The AMB exciter is integrated in the overall measurement set-up by means of a convenient interface to the standard mathematical program package MATLAB [5]. It provides the following functions to the experimenter:

- AMB control: Start, stop, load controller parameters
- set excitation parameters
- read variables from the DSP
- trace the time history of variables from the DSP

Excitation and force computation

In contrast to conventional bearing applications, the controlled variable is the force rather than the displacement. The displacement can be considered mainly as a disturbance input. The main requirement to the AMB is that the force can be accurately set and - most importantly - accurately *measured*, i.e., computed from appropriate measurements.
In particular, the force measurement must not be corrupted by

- iron saturation, eddy currents, hysteresis, sensor and actuator dynamics
- manufacturing inaccuracies (rotor diameter), for operation with different rotors
- misalignment (for operation in roller bearings mounted on the flexible foundation).

Moreover, it must be accurate when

- the rotor is displaced by the excitation
- there is a bias force (for supporting the rotor with AMB's).

The mechanical set-up itself (elastic, rotating structure combined with elastic, non-rotating structure) gives rise to various higher harmonics and combinations of both excitation and rotation frequency. Therefore, it is important that the excitation is guaranteed to be purely sinusoidal.
The force can be computed in different ways from different measured variables (magnetic fluxes, coil currents, coil voltages, rotor position). Since the accuracy of this force computation is crucial for the project, there is a need to establish an accurate non-linear, two-dimensional model of the magnetic bearing. This will be used to compare the accuracy of different ways of force measurement. Moreover, the underlying model motivates the algorithm proposed in section 4.

3. MODELS OF JOURNAL BEARINGS

3.1. Some different geometries

Figure 2 shows the standard geometries a) and b) as well as a generalized geometry that is used for the described AMB exciter.

In configuration a), the pole pairs are magnetically well separated from each other. There is therefore almost no flux between the pole pairs. The absolute value of the force is then about equal for the two poles of one pole pair. The pole pairs y_p, y_n do not exert a force in x direction on the rotor, and *vice versa*. Analytical modelling of this configuration is straight-forward. It is explained in section 3.3.

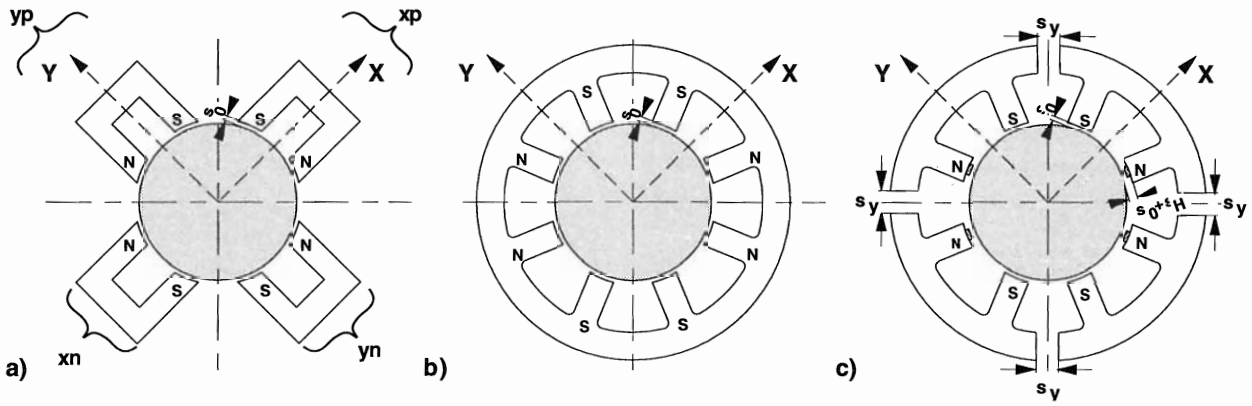

FIGURE 2: Schematic diagrams of different geometries for radial magnetic bearings: a) with well-separated pole pairs, b) with fully coupled pole pairs, and c) a more general model with more or less decoupled pole pairs and different nominal air gaps for the north and south poles. Geometry c) has been realised.

In most applications, however, configuration b) is used. This configuration has significant constructive advantages over configuration a). The magnetic pole pairs are mechanically and magnetically well connected through a yoke. This magnetic coupling influences the flux distribution and thus the resulting force on the rotor, F(x,i), significantly and should therefore be taken into account. This can be done by modelling the radial bearing as a network of magnetic resistors. The flux distribution and the resulting force can then be computed as a function of the coil currents and the rotor position. This is done in section 3.4. However, the solution of the resulting simultaneous equations involves the inversion of an 8*8 matrix. It is therefore not so easy to obtain exact results in closed form.

Configuration c) is the realised set-up of the magnetic bearing exciter. Flux sensors are placed at all north poles. Therefore, the air gaps are larger at the north poles than at the south poles. To reduce the magnetic coupling, the pole pairs are separated. This represents a compromise between magnetic decoupling and constructional advantages. For a comparison between the different set-ups, the reader is referred to section 4.

The magnetic resistor model is established for configuration c). Configurations a) and b) are special cases of this.

3.2. Preliminaries

Both models proposed in this section have the following restrictions:

- Saturation is neglected
- The surface of the magnetic poles is assumed to be plain. (The effect of the curvature of the pole surfaces in geometry a) has been studied in [6].)
- Only static forces are considered
- Winding numbers and cross sections for all poles are equal (as it is usually the case)

Notation. The variables are illustrated in figure 3.

r_x, r_y rotor displacement in x and y direction

s air gap

A cross section of the magnetic poles

i coil current

N winding number of a pole pair

Let $(.)_{xp}$, $(.)_{yp}$, $(.)_{xn}$, $(.)_{yn}$ refer to the pole pairs at positive and negative x and y axis, respectively;

$(.)_N$, $(.)_S$ to north and south pole, respectively

Thus, for instance, s_{xpN} denotes the air gap at the north pole of pole pair xp.

s_H additional air gap for flux sensor in config. c)

s_y air gap between pole pairs in configuration c)

l_s length of magnetic pole

l_y length of yoke between the magnetic poles

a half the angle between two adjacent magnetic poles

Φ magnetic flux

B magnetic flux density

H magnetic field

V magnetic potential difference

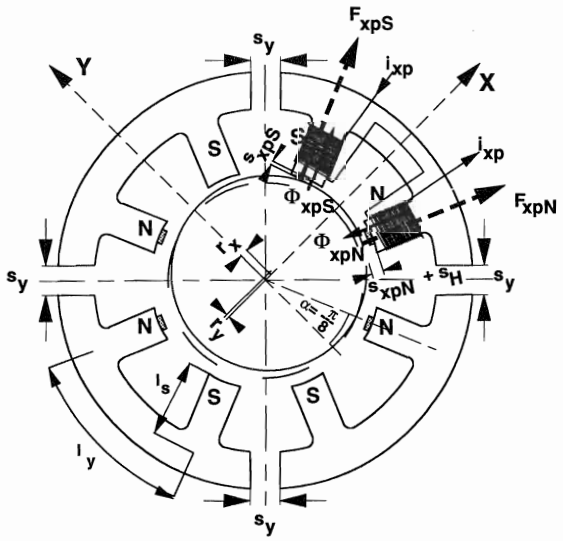

FIGURE 3: Configuration from figure 2.c) with illustration of the used variables. Not to scale.

Geometry. With $\alpha = \pi/8$ we find from simple geometry:

$$\begin{aligned}
s_{xpN} &= s_0 - r_x\cos\alpha + r_y\sin\alpha \\
s_{xpS} &= s_0 - r_x\cos\alpha - r_y\sin\alpha \\
s_{ypS} &= s_0 - r_x\sin\alpha - r_y\cos\alpha \\
s_{ypN} &= s_0 + r_x\sin\alpha - r_y\cos\alpha \\
s_{xnN} &= s_0 + r_x\cos\alpha - r_y\sin\alpha \\
s_{xnS} &= s_0 + r_x\cos\alpha + r_y\sin\alpha \\
s_{ynS} &= s_0 + r_x\sin\alpha + r_y\cos\alpha \\
s_{ynN} &= s_0 - r_x\sin\alpha + r_y\cos\alpha
\end{aligned} \tag{3.2.1}$$

3.3. Analysis of configuration a)

We neglect the small magnetic coupling between the pole pairs, which is equivalent to setting $s_y = \infty$. Thus, $\Phi_{xp} = \Phi_{xpN} = \Phi_{xpS}, F_{xpN} = F_{xpS}$ *etc.* Further we neglect the magnetic resistance of the iron. The resulting magnetic force F_x in the x-direction can then be calculated from the following equations:

$$F_x = 2\cos\alpha\cdot\left(F_{xpN} - F_{xnN}\right) \tag{3.3.1}$$

$$F_{xpN} = \frac{\Phi_{xp}^{\,2}}{2A\cdot\mu_0}; \quad F_{xnN} = \frac{\Phi_{xn}^{\,2}}{2A\cdot\mu_0} \tag{3.3.2}$$

$$\Phi_{xp} = \frac{N\cdot i_{xp}}{s_{xpN}+s_{xpS}}\cdot A\cdot\mu_0; \quad \Phi_{xn} = \frac{N\cdot i_{xn}}{s_{xnN}+s_{xnS}}\cdot A\cdot\mu_0 \tag{3.3.3}$$

as shown in [7]. With (3.2.1), we get

$$\begin{aligned}
s_{xpN} + s_{xpS} &= 2\left(s_0 - r_x\cos\alpha\right) \\
s_{xnN} + s_{xnS} &= 2\left(s_0 + r_x\cos\alpha\right)
\end{aligned} \tag{3.3.4}$$

Combining (3.3.1-3.3.4) yields

$$F_x = \cos\alpha\cdot\frac{K}{4}\left(\frac{i_{xp}^{\,2}}{\left(s_0 - r_x\cos\alpha\right)^2} - \frac{i_{xn}^{\,2}}{\left(s_0 + r_x\cos\alpha\right)^2}\right) \tag{3.3.5}$$

where $K = N^2 A\mu_0$

or, with

$$i_{xp} = i_0 + i_x; \quad i_{xn} = i_0 - i_x \tag{3.3.6}$$

$$F_x = \cos\alpha\cdot\frac{K}{4}\left(\frac{\left(i_0 + i_x\right)^2}{\left(s_0 - r_x\cos\alpha\right)^2} - \frac{\left(i_0 - i_x\right)^2}{\left(s_0 + r_x\cos\alpha\right)^2}\right)$$

We can linearise this equation to

$$F_x = k_s\cdot r_x + k_i\cdot i_x \tag{3.3.7}$$

where

$$k_s = \left.\frac{dF_x}{dr_x}\right|_{r_x=0,i_x=0} = \frac{K\,i_0^{\,2}}{s_0^{\,3}}\cos^2\alpha \tag{3.3.8}$$

$$k_i = \left.\frac{dF_x}{di_x}\right|_{r_x=0,i_x=0} = \frac{K\,i_0}{s_0^{\,2}}\cos\alpha \tag{3.3.9}$$

$$\frac{k_s}{k_i} = \frac{i_0}{x_0}\cos\alpha \tag{3.3.10}$$

As stated above, the force in y direction is computed independently in the same way.

3.4. Analysis of radial magnetic bearings by two-dimensional modelling as network of magnetic resistors

The radial bearing can be modelled as a network of magnetic resistors, as shown in the equivalent network diagram in fig. 4. This method is less accurate than FE modelling but gives considerable insight into the behaviour of magnetic bearings.

The magnetic resistance is defined as the ratio of mag-

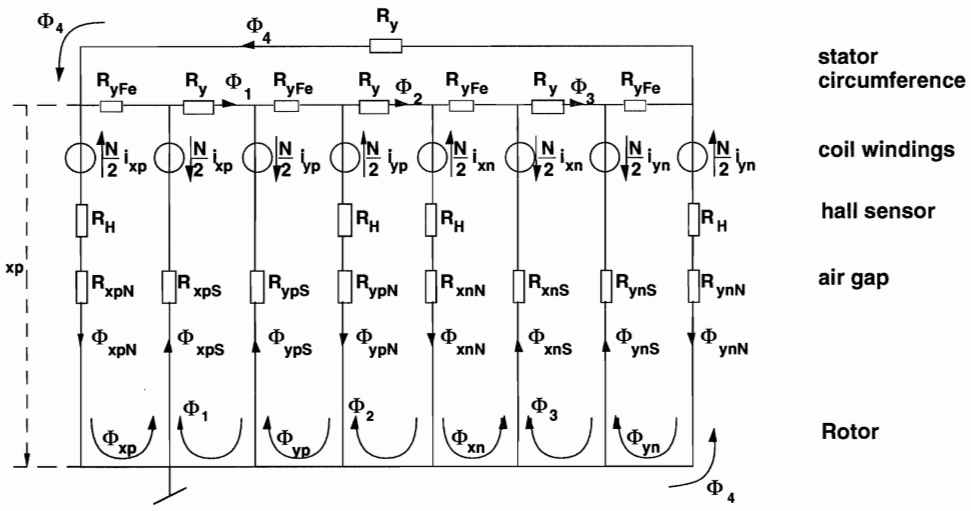

FIGURE 4: Equivalent network diagram

netic potential difference ΔV and magnetic flux Φ,

$$R = \frac{\Delta V}{\Phi} = \frac{\int Hds}{\Phi} \qquad (3.4.1)$$

The magnetic resistance of the different air gaps is given by

$$R_{sxpN} = \frac{s_{xpN}}{\mu_0 A},\ etc.,\ R_H = \frac{s_H}{\mu_0 \cdot A},\ R_{sy} = \frac{s_y}{\mu_0 \cdot A} \qquad (3.4.2)$$

The magnetic resistance of the iron can be accounted for by writing

$$R_{xpN} = R_{sxpN} + \frac{l_s}{\mu_0 \mu_r A},\ etc.,\ R_y = R_{sy} + \frac{l_y - s_y}{\mu_0 \mu_r A},\ \text{and}$$

by introducing

$$R_{yFe} = \frac{l_y}{\mu_0 \mu_r A}$$

We can now find the flux distribution as a function of the coil currents and the air gaps using standard methods of electric circuit theory: Let

$$\Phi_z = \begin{bmatrix} \Phi_{xp} \\ \Phi_{yp} \\ \Phi_{xn} \\ \Phi_{yn} \\ \hline \Phi_1 \\ \Phi_2 \\ \Phi_3 \\ \Phi_4 \end{bmatrix}, \quad U_m = N \cdot \begin{bmatrix} i_{xp} \\ i_{yp} \\ i_{xn} \\ i_{yn} \\ \hline (i_{xp} - i_{yp})/2 \\ (i_{xn} - i_{yp})/2 \\ (i_{xn} - i_{yn})/2 \\ (i_{xp} - i_{yn})/2 \end{bmatrix} \qquad (3.4.3,4)$$

Φ_z is a vector of eight linearly independent circular fluxes (Φ_{xp}, ... are the main fluxes, Φ_1 ... Φ_y are auxiliary quantities; see fig. 4). U_m is the vector of the related sources of magnetic potential difference (amp turns).

Then Φ_z is given by

$$\Phi_z = Z^{-1} \cdot U_m \qquad (3.4.5)$$

where the impedance matrix Z is defined by equation (3.4.7), see below.

The flux at the magnetic poles is given from the elements of Φ_z. Now we can compute the force at each magnetic pole with (*cf.* 3.3.2)

$$F_{(.)} = \frac{\Phi_{(.)}^2}{\mu_0 A} \qquad (3.4.6)$$

and build the vector sum of the pole forces to obtain the resulting force. (Index (.) refers to the magnetic poles xpn, *etc.*.)

Comparison with previous results. . Configuration a) is a special case of configuration c) with "large" s_y , and $s_H = 0$. By letting $s_y = \infty$, and neglecting the magnetic resistance of the iron, the results of the proposed network method coincide exactly with (3.3.5) for all rotor displacements and coil currents, as expected.

3.5. An extra result: The parameter k_s for configuration b)

Configuration b) is a special case of configuration c) with $s_y = 0$, $s_H = 0$. It is found that there is a flux between the pole pairs as soon as the rotor is displaced from its nominal position (*cf.* fig. 3.6.1). However, there is no flux between the pole pairs as long as the rotor is in its nominal position.

For the linearisation of the characteristic curve at $r_x = r_y = 0,\ i_x = i_y = 0,$

$$F_x = k_s \cdot r_x + k_i \cdot i_x \qquad (3.3.7)$$

the following must be noted:

- k_s: k_s is exactly

$$k_s = \left.\frac{dF_x}{dr_x}\right|_{r_x=0, i_x=0} = \frac{K i_0^2}{s_0^3} \qquad (3.5.1)$$

$$Z = \left[\begin{array}{cccc|cccc} R_{xpN}+R_{xpS}+R_H+R_{yFe} & 0 & 0 & 0 & +R_{xpS} & 0 & 0 & R_{xpN}+R_H \\ 0 & R_{ypN}+R_{ypS}+R_H+R_{yFe} & 0 & 0 & -R_{ypS} & -R_{ypN}-R_H & 0 & 0 \\ 0 & 0 & R_{xnN}+R_{xnS}+R_H+R_{yFe} & 0 & 0 & +R_{ynN}+R_H & +R_{xnS} & 0 \\ 0 & 0 & 0 & R_{ynN}+R_{ynS}+R_H+R_{yFe} & 0 & 0 & -R_{ynS} & -R_{ynN}-R_H \\ \hline +R_{xpS} & -R_{ypS} & 0 & 0 & R_{xpS}+R_{ypS}+R_y & 0 & 0 & 0 \\ 0 & -R_{ypN}-R_H & +R_{ynN}+R_H & 0 & 0 & R_{ypN}+R_{xnN}+R_y+2R_H & 0 & 0 \\ 0 & 0 & +R_{xnS} & -R_{ynS} & 0 & 0 & R_{xnS}+R_{ynS}+R_y & 0 \\ R_{xpN}+R_H & 0 & 0 & -R_{ynN}-R_H & 0 & 0 & 0 & R_{xpN}+R_{ynN}+R_y+2R_H \end{array}\right] \qquad (3.4.7)$$

Equation (3.4.7)

while modelling with separate pole pairs (config. a) yields

$$k_s = \left.\frac{dF_x}{dr_x}\right|_{r_x=0,i_x=0} = \frac{K i_0^2}{s_0^3}\cos^2\alpha \qquad (3.3.8)$$

This is a difference of 17%. It is thus clear that the two-dimensional network model is necessary for a correct calculation of k_s in the usual radial bearing geometry b). This result has been found analytically, using the program Mathematica.

- k_i is equal for the geometries a) and b):

$$k_i = \left.\frac{dF_x}{di_x}\right|_{r_x=0,i_x=0} = \frac{K i_0}{s_0^2}\cos\alpha \qquad (3.3.9)$$

Thus, in contrast to (3.3.10),

$$\frac{k_s}{k_i} = \frac{i_0}{x_0}\cdot\frac{1}{\cos\alpha} \qquad (3.5.2)$$

As to the non-linear formula, it is obvious from this that (3.3.5) is not true.

$$F_x = \cos\alpha\cdot\frac{K}{4}\left(\frac{i_{xp}^2}{(s_0 - r_x/\cos\alpha)^2} - \frac{i_{xn}^2}{(s_0 + r_x/\cos\alpha)^2}\right) \qquad (3.5.3)$$

is found to be a good approximation for small rotor displacements.

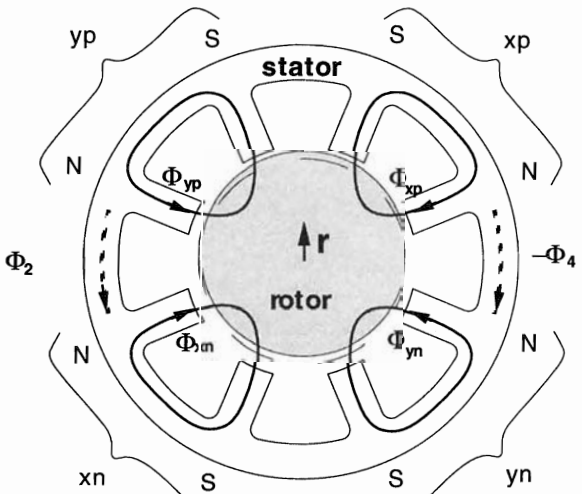

FIGURE 5: Flux in a radial bearing with rotor displacement r, when the coil currents are equal at all poles. Solid: Main flux Φ_{xp}, Φ_{yp}, Φ_{xn}, Φ_{yn}; dashed: Flux between the pole pairs, Φ_2 and Φ_4

3.6 Results for configuration c)

For the asymmetric configuration c, there is a large flux between the pole pairs when the pole pairs are connected (s_y=0). This is the case unless the rotor is in nominal position *and* the coil currents are all equal. If s_y is reasonably large (*i.e.* 10*s0), $\Phi_{y,(.)}$ becomes small. However, it must, and can, be taken into account for a precise force computation. Further details are given in section 4.2.

4. CONFIGURATIONS AND METHODS FOR FORCE MEASUREMENT

4.1 Possibilities

For the purpose given, different configurations have been considered. We mention three of them:

1) The exerted force can be computed from the coil currents and displacement. This can be done with configuration a) using equation (3.3.5) applied for x and y direction, or with configuration b) using equation (3.5.2)
   This estimate cannot take into account iron saturation nor eddy currents and hysteresis effects which dynamically counteract the control current.
2) Alternatively, the force can be computed from measurement of the magnetic flux in all poles of the radial bearing, using (3.4.7) for each magnetic pole. In this way, saturation, eddy current and hysteresis effects are taken into account. However, the flux sensors must be inserted into the air gap. The air gap must therefore be widened by the thickness of the sensor, *i.e.*, about 1mm. This increases the required ampere turns (amplifier power) significantly. Furthermore, the hardware complexity is increased as 16 extra analog inputs are required.
3) The force can be computed from flux measurement in all magnetic north poles only, as in configuration 2). In this way, eddy current and hysteresis effects are taken into account. The required ampere turns as well as the hardware complexity are increased only half as much as in version 2), while the system retains all it's advantages over version 1). The bearings become asymmetric, as the air gap of the north poles is 1mm wider than at the south poles. To reduce undesirable effects of this asymmetry on the flux distribution (*cf.* section 3.7), the pole pairs must be separated by a sufficiently large air gap s_y.

Configuration 3) is an optimal compromise with respect to accuracy, hardware complexity and amplifier power requirements. It has been realised with s_0 = 0.8 mm,, s_H = 1 mm, and s_y = 16 mm.

4.2 Force computation from Φ_N in configuration 3)

With the (inaccurate) assumption that $\Phi_N = \Phi_S$ and s_y = 16mm, computing the resulting force from equation (3.4.6) does not give the desired accuracy.

Certainly, Φ_S can be computed from Φ_N, the coil currents and the rotor position. This problem is actually even over-determined. However, this computation must be applicable in real time at sampling times of some 100 µs. Moreover, its results should not be corrupted by

iron saturation, actuator dynamics, *etc.* Therefore the following algorithm is proposed:

1) Assume $\Phi_S=\Phi_N$ for all pole pairs.

First iteration:

2) Compute magnetic potentials V_{xp}, V_{yp}, V_{xn}, V_{yn} on the stator yokes from the pole fluxes and rotor position (magnetic resistance of air gap)

$$\left.\begin{aligned} V_{xp}^{(1)} &= \Phi_{xpN}\left(R_{xpN}+R_H\right)-\Phi_{xpN}\cdot R_{xpS} \\ V_{yp}^{(1)} &=\ldots, V_{xn}^{(1)} =\ldots, V_{yn}^{(1)} =\ldots, \end{aligned}\right\} \quad (4.2.1)$$

3) Compute flux $\Phi_{1..4}$ from this

$$\left.\begin{aligned} \Phi_1^{(1)} &= (V_{xp}^{(1)} - V_{yp}^{(1)})/R_y \\ \Phi_2^{(1)} &= \ldots., \ldots. \end{aligned}\right\} \quad (4.2.2)$$

4) Compute non-measured flux Φ_S in south poles

$$\left.\begin{aligned} \Phi_{xpS}^{(1)} &= \Phi_{xpN}+\Phi_1-\Phi_4 \\ \Phi_{ypS}^{(1)} &=\ldots, \ldots \end{aligned}\right\} \quad (4.2.3)$$

5) Second iteration: repeat steps 2)...4) if better accuracy is desired.

6) Apply equation (3.4.6) to compute the force.

The results of this algorithm have been verified against the exact force computation as given in section 3.4. The comparison is shown in figure 6.

5. CONTROL CONCEPT

The AMB system must be able to support the rotor and at the same time to excite it. The frequency Ω of the excitation is set by the experimenter, as well as the amplitudes A and relative phase shifts ϕ of the forces at the four bearing axes. The controller must ensure that the harmonic part of the bearing force at frequency Ω exactly matches these parameters.
This requires force control. At the same time, stability must be maintained by position feedback. The position controller clearly counteracts the force controller, unless it has a transmission zero (notch filter) exactly at the user-defined excitation frequency. The amplitudes and relative phase shifts that are prescribed would therefore not be faithfully transmited but distorted by the position controller.

The problem is solved with the multi-loop controller structure as shown in figure 7:

- The innermost loop is governed by a force controller C_F. Its goal is that the bearing force F is equal to its input force F_{des}. Thereby, $F=F(B,x)$ is computed with the algorithm outlined in section 4.2, thus accounting for the non-linearities in the bearing.
- The next loop is the position control loop. The position controller $C_x(s)$ sets F_x such that the plant is kept stable.
- So far, F_{des} is clearly not equal to the desired force, F_Ω, at frequency Ω. This is due to the above-mentioned disturbance. Therefore, an adaptation loop is added that compensates this distortion at the excitation frequency. This problem is much the same as

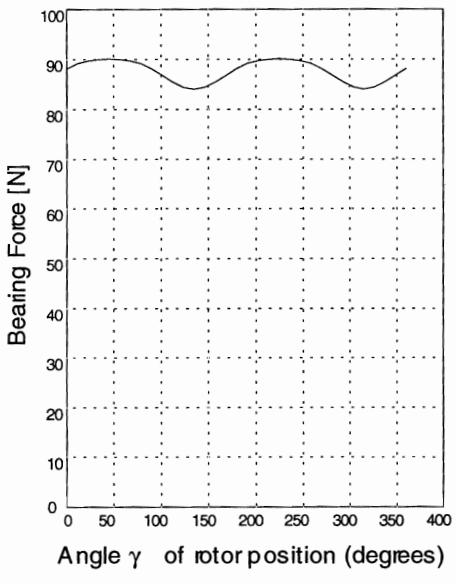

a)

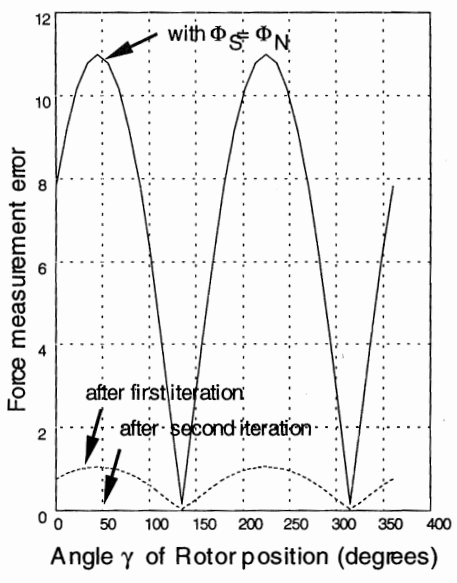

b)

FIGURE 6: Force exerted by the AMB on the rotor along a circular path $r_x = \Delta*\cos\gamma$, $r_y = \Delta*\sin\gamma$, where $\Delta = 0.2*s_0$. a) bearing force (absolute value); b) accuracy of force computation (absolute value) after step 1 (solid), after the first iteration (dashed), and after the second iteration (dotted) of the force computation algorithm. After the second step of the algorithm, the remaining error is negligible.

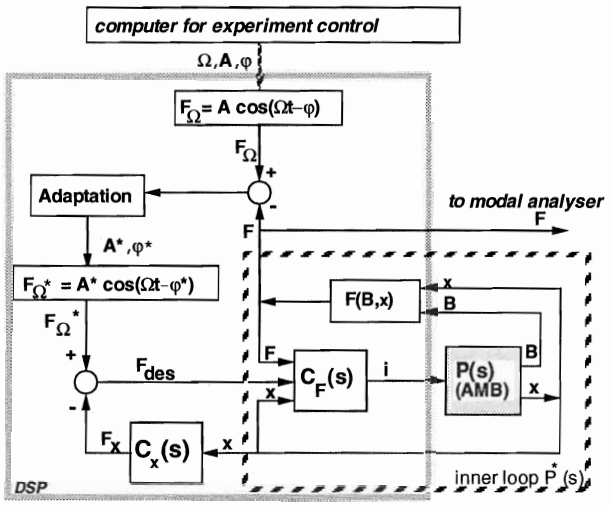

FIGURE 7: Controller architecture

unbalance control. The difference lies in the fact that the synchronous component of the force must be a non-zero, user-defined value. Therefore, "feed-forward" methods developed for unbalance control can be applied.

The key idea with feed-forward unbalance compensation is that a sinusoidal signal is fed into the loop. Its parameters (amplitude and phase angle) are adapted until the error signal which enters the adaptation block is zero at the considered frequency. This has certain advantages in comparison with linear notch-filter techniques. The method is described in detail in [8,9].

6. CONCLUSIONS

An AMB system for accurately generating excitation forces and at the same time stabilising a rotor with AMBs has been developed. This set-up uses flux sensors, a novel two-dimensional magnetic bearing model for force measurement, and a novel multi-loop controller architecture for force control. The modelling method has been shown to be important for all applications with the widely used radial bearing geometry in Figure 2.c).

ACKNOWLEDGEMENTS

The project is funded by the European Community and the Swiss Government. We wish to thank the staff from Mecos Traxler as well as Ladislav Kucera for many helpful discussions and contributions. Philipp Bühler has contributed valuable hardware controller developments.

REFERENCES

1. Xu J., Gasch R.: Kleiner Beitrag zur Behandlung linearer periodisch zeitvarianter Bewegungsgleichungen. Bericht aus dem Institut für Luft- und Raumfahrt der Techn. Univ. Berlin, IRL-Mitteilungen 278, 1993
2. Nordmann, R.: Identification Techniques in Rotordynamics. Symposium on Diagnostics of Rotating Machines in Power Plants, Udine, 1993
3. Ulbrich, H.: New Test Techniques Using Magnetic Bearings. Magnetic Bearings, Proceedings of the First International Symposium, June 6-8, Zurich, Switzerland
4. Nordmann, R., Matros, M., Neumer, T.: Parameter Identification in Rotating Machinery by Means of Active Magnetic Bearings. IFTOMM, 4th Conference on Rotor Dynamics, Chicago, Illinois, 1994
5. Herzog, R., Siegwart, R.: High Performance Data Acquisition, Identification, and Monitoring for Active Magnetic Bearings. 2nd Int. Symp. on Magnetic Suspension Technology, NASA, Seattle/USA, Aug. 11-13,1993
6. Knight, J.D., Xia, Z., McCaul, E. B.: Forces in Magnetic Bearings: Non-linear Computation and Experimental Measurement. Proc. Third Int. Symp. on Magnetic Bearings, July 29-31, Alexandria VA, USA, 1992
7. Schweitzer, G., Traxler, A., Bleuler, H.: Active Magnetic Bearings. Verlag der Fachvereine, Zurich, Switzerland, 1994
8. Larsonneur, R., Siegwart, R., Traxler, A.: Active Magnetic Bearing Control Strategies for Solving Vibration Problems in Industrial Rotor Systems. Proceedings of the 5th International Conference in Rotating Machinery (IMechE), University of Bath (UK), September 7-10, 1992
9. Larsonneur, R., Herzog, R.: Feedforward compensation of unbalance: New Results and Application Experiences. IUTAM Symposium *The Active Control of Vibration*, Univ. of Bath, UK, September 5-8, 1994 (to appear)